Experimental study of an in-fiber acousto-optic tunable bandpass filter for single- and dual-wavelength operation in a thulium-doped fiber laser

E. Hernández Escobar,[1] M. Bello Jiménez,[1,*] A. Camarillo Avilés,[1] R. López Estopier,[1,2] O. Pottiez,[3] M. Durán Sánchez,[2,4] B. Ibarra Escamilla,[4] and M. V. Andrés[5]

[1]*Instituto de Investigación en Comunicación Óptica (IICO), Universidad Autónoma de San Luis Potosí, Av. Karakorum No. 1470 Lomas 4ª Secc., 78210, San Luis Potosí, Mexico*
[2]*Consejo Nacional de Ciencia y Tecnología (CONACYT), Av. Insurgentes Sur No. 1582, Col. Crédito Constructor, Del. Benito Juárez, México, 039040, D.F., Mexico*
[3]*Centro de Investigaciones en Óptica (CIO), Loma del Bosque No. 115, Col. Lomas del Campestre, 37150, León, Guanajuato, Mexico*
[4]*Instituto Nacional de Astrofísica, Óptica y Electrónica (INAOE), Luis Enrique Erro No 1, Departamento de Óptica, 72000 Puebla, Mexico*
[5]*Universidad de Valencia, Departamento de Física Aplicada y Electromagnetismo, ICMUV, c/Dr. Moliner 50, Burjassot, 46100 Valencia, Spain*
*miguel.bello@uaslp.mx

Abstract: A tunable single- and dual-wavelength thulium-doped all-fiber laser is demonstrated based on the implementation of an in-fiber acousto-optic tunable bandpass filter (AOTBF). The AOTBF is fabricated to be operated in the 1.9 μm region, and takes advantage of the intermodal coupling effect produced by traveling flexural acoustic waves in an optical fiber. It exhibits a 3-dB bandwidth of 2.04 nm with an insertion loss of 4.75 dB. The tuning properties of the AO device allows a continuous-wave operation with characteristics of wide tuning range (211.5 nm), narrow linewidth (50 pm) and high signal-to-noise ratio (60 dB). In the dual-wavelength regime, the laser is capable of independent tuning of each of the laser lines, achieving a tunable dual-wavelength emission that extends from 1802.67 to 1932.75 nm. A controllable wavelength spacing with minimum and maximum separations of 1.04 and 130.08 nm is obtained.

1. Introduction

Dual-wavelength fiber lasers with characteristics of narrow linewidth, high stability and broadband tunability are very attractive optical sources with applications in many research fields such as THz radiation [1–3], coherent anti-Stokes Raman scattering [4], optical sensing [5] and high-speed communication systems [6], among others. Currently, and derived from the growing interest in developing all-fiber devices for the 2-micron wavelength region, various approaches of dual-wavelength thulium-doped fiber lasers (TDFLs) have been proposed and demonstrated based on the inclusion of different types of fiber-optic components, such as fiber Bragg gratings (FBGs) [7–9], Mach-Zehnder interferometers [10–12], tunable filters [12–14], and Sagnac loops [15–19], among others, all of them offering the advantages of high stability and easy implementation. Notwithstanding, from a practical point of view, most of these approaches require of arbitrary adjustments of polarization controllers (PCs) or variable optical attenuators (VOAs), which impose limitations in terms of repeatability and reliability. For these reasons, and despite the

recent progress in this field, it is worthwhile to investigate alternative solutions to achieve a tight control over the cavity parameters and enable improvements on dual-wavelength generation.

In recent years, all-fiber acousto-optic (AO) devices based on flexural acoustic waves have received a great deal of attention due to their properties of wide tuning range [20–23], bandpass filtering [24–30], AO mode conversion [31–35], high resolution and accuracy [36–40]. The operation principle of these AO devices relies on the intermodal coupling between core (LP_{01}) and some specific cladding modes ($LP_{1,m}$ family) when a flexural acoustic wave propagates along an uncoated section of optical fiber. This AO effect has been demonstrated to be a useful mechanism to bypass an obstacle at the core via cladding propagation and the subsequent recoupling to the core at the end of the interaction length. Based on this property, this type of AO device can be designed as an efficient tunable bandpass filter [24,26,29,30]. Among these schemes, our group has proposed an AO tunable bandpass filter (AOTBF) consisting of a section of coreless optical fiber as the core-mode blocker (CMB) [29,41]. In this work, the filter capabilities are investigated as a dual-wavelength filtering device biased by two simultaneous acoustic signals. In this manner, the AOTBF undergoes a dual-wavelength bandpass transmission that is controlled by the amplitude and frequency of the incident acoustic signals. Based on this approach, the AOTBF is proposed as a dual-wavelength filtering device to perform a precise control of the cavity loss and provide a stable and tunable dual-wavelength emission in a thulium-doped fiber laser.

In this paper initial experiments are focused on determining the conditions and characteristics of the AOTBF to be operated in the thulium emission band, and its capacity as a single- or dual-wavelength filter is analyzed in a continuous-wave (CW) TDFL. Narrow linewidths around 50 pm and a fine-tuning range from 1757.6 to 1969.1 nm is observed, demonstrating the potential of this type of AO device to realize an efficient single- or dual-wavelength generation near the 2 micron region. These results, to the best of our knowledge, are the first demonstration of an in-fiber AO tunable bandpass filter for dual-wavelength operation. Its capacity to be operated by two independent acoustic signals allows a precise control of dual-wavelength emission, such as tuning range and wavelength separation, which depends on regulating the amplitude and frequency of the input signals.
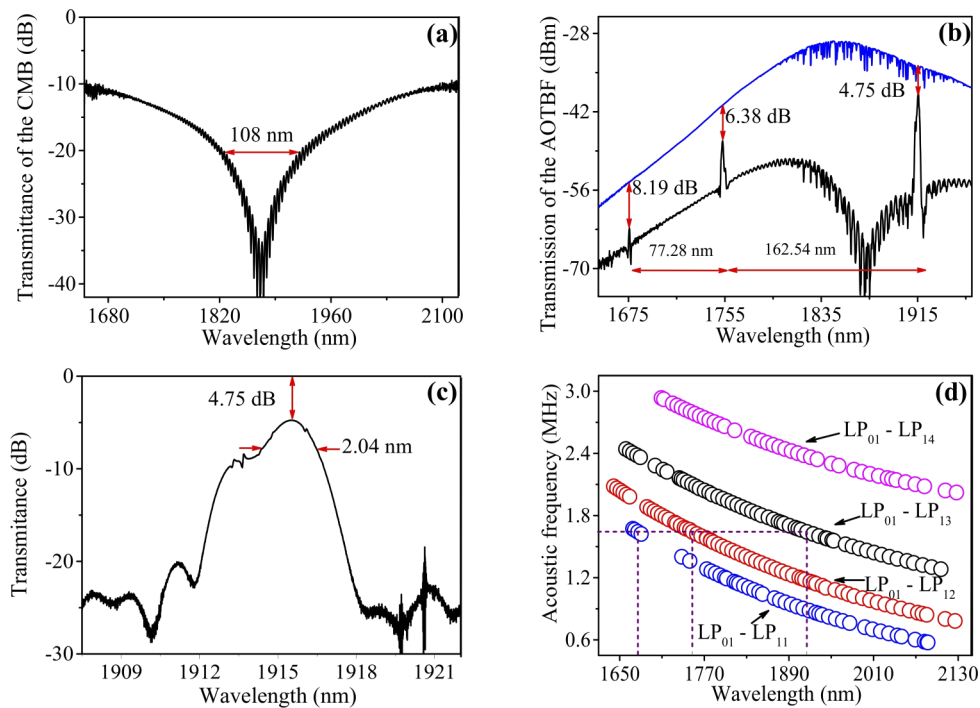
2. The AOTBF

The schematic setup of the acousto-optic tunable bandpass filter (AOTBF) is illustrated in Fig. 1. The acousto-optic effect that governs the operation principle of the AOTBF is the intermodal coupling between the core mode and some specific cladding modes in the fiber. Because of the characteristics of the acoustic modes of a standard optical fiber, the easiest and most efficient solution is to exploit the flexural acoustic waves [42]. The filter is composed of two independent signals sources, labeled as S_1 and S_2, which are combined and amplified to drive a 20-mm ceramic piezoelectric disk (PD). An aluminum concentrator horn is attached to the PD and it focuses the acoustic vibration into the fiber through its tip. In order to prevent the attenuation of the acoustic wave, the optical fiber is stripped from the outer polymer jacket. The total length L of the fiber consist of three sections specified as L_1, d and L_2. The filter is fabricated following the same process described in Ref. [29], but in this case the core-mode blocker (CMB) is especially suited for the AOTBF to be operated in the thulium emission band. The length of fiber L_1 is used to achieve the intermodal coupling between core and cladding modes previous the CMB. The purpose of the CMB, which is formed by a section d of coreless optical fiber (Thorlabs FG125LA), is to attenuate the optical wavelengths that do not fulfill the phase-matching condition and continue to be guided by the core. Hence, only the resonant wavelengths, that satisfy the phase-matching condition and are coupled to a cladding mode, propagate along the CMB with a negligible perturbation via cladding propagation. At the final stage of AO interaction, L_2 is chosen to reach a full mode recoupling cycle to the core mode. In this sense, the filter performs

dynamical bandpass transmission response that depends on the amplitude and frequency of the incident acoustic waves. The lengths L_1 and L_2 of the optical fibers (SMF-28) were selected as 24 and 34.3 cm, respectively, where section L_2 is chosen longer than L_1 in order to compensate the attenuation of the acoustic wave and maximize the transmittance [29]. The CMB has a length of 1.8 mm. This length was optimized experimentally and it produces attenuations higher than 34.4 dB around the 1875 nm region. Finally, in order to avoid undesired acoustic reflections, the outer polymer jacket of the fiber is used as damper. It efficiently attenuates the acoustic wave at both ends of the filter structure.
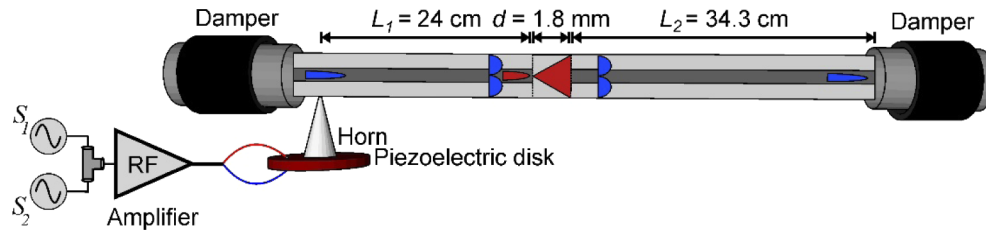
Fig. 1. Experimental setup of the AOTBF.

The transmittance spectrum of the CMB is shown in Fig. 2(a). For this measurement, an amplified spontaneous emission (ASE) source based on a thulium-doped fiber (TDF) is used to illuminate the AOTBF in the absence of acoustic wave. The transmittance spectrum is measured with an optical spectrum analyzer (OSA, Yokogawa AQ6375 with 50 pm of wavelength resolution) by means of the difference between ASE spectrum and spectral response of the CMB. A broad and deep attenuation notch is observed with 34.4 dB of maximum attenuation centered at 1874.41 nm. Moreover, assuming attenuation values higher than 20 dB, a broad attenuation bandwidth of 108 nm is measured for a range wavelengths between 1820.41 and 1928.41 nm. On the other hand, by switching one of the acoustic signals on, only the resonant wavelengths are able to bypass the attenuation of the CMB via cladding propagation. This phenomenon is shown in Fig. 2(b) when applying a sinusoidal signal of 1.642126 MHz and 33 V (hereinafter the voltage is a peak-to-peak measurement) to drive the PD. One can observe three peaks of bandpass transmission that correspond to $LP_{01}-LP_{11}$, $LP_{01}-LP_{12}$ and $LP_{01}-LP_{13}$ intermodal couplings, exhibiting a resonant optical wavelength (λ_R) of 1675.62, 1752.9 and 1915.44 nm, respectively. In this measurement, a low-amplitude intensity modulation is also observed in the transmission spectrum, this effect is probably caused by some interferometric effect produced by reflections between the OSA detector and the fiber connector when the measurement was carried out. For this particular setup, and as a result of the nonflat frequency response of the PD, the maximum transfer of energy occurs for the $LP_{01}-LP_{13}$ intermodal coupling. For comparison purposes, the ASE spectrum (blue curve) is also included in the figure. The fine structure around 1900 nm is demonstrated to be caused by the molecular resonances of H_2O and CO_2 in air [43]. A detailed view of the strongest resonance is shown in Fig. 2(c), where a 3-dB optical bandwidth of 2.04 nm and a minimum insertion loss of −4.75 dB is measured. This high insertion loss is likely to be caused by the attenuation of the acoustic wave and the losses that the splices of the CMB introduce in both the cladding mode and the acoustic wave. The calibration curves of the device, i.e., the acoustic wave frequency (f_a) versus the shift of λ_R, is shown in Fig. 2(d) for four different intermodal couplings. This last result indicates the required frequencies for the AOTBF to be operated in the thulium emission band, covering a range of acoustic frequencies from 0.575126 to 2.934126 MHz that corresponds to a wide span of resonant optical wavelengths from 1641.4 to 2127.6 nm. The dashed line in Fig. 2(d) indicates the strongest intermodal coupling at the acoustic frequency of 1.642126 MHz.

Fig. 2. (a) Transmittance spectrum of the CMB centered at 1874.41 nm. (b) ASE (blue line) and spectral response of the AOTBF at the acoustic frequency of 1.642126 MHz (black line). (c) Close-up view of the strongest resonance. (d) Shift of the acoustic frequency versus resonant optical wavelength.

In the next section, taking as a reference the calibration of the AOTBF, it is proposed as an alternative single- or dual-wavelength filtering device to perform a precise control of the cavity loss and provide a stable and tunable dual-wavelength emission in a thulium-doped fiber laser.

3. Laser setup and experimental results

A schematic view of the all-fiber laser is shown in Fig. 3. It comprises a ring cavity with a 3-m long thulium-doped fiber (TDF, CorActive SCF-TM-8/125) as the gain medium. The TDF is pumped through a 1550/2000 nm wavelength division multiplexer (WDM) by a fiber laser source emitting at 1568 nm providing 1.73 W of maximum pump power. Following a counterclockwise sense, a 50/50 fiber coupler is spliced to the WDM. One port of the coupler is used to provide the laser output, and the remaining port is spliced to an in-line polarization controller (PC). The PC is added in order to adjust the polarization state previous the AOTBF. A fiber isolator (ISO) is connected after the filter, and it was used to force unidirectional operation within the cavity. Finally, the ring cavity is closed by connecting the transmission port of the ISO with the TDF.

3.1. Single-wavelength operation

Initial experiments were carried out in order to investigate the laser performance assuming the case of maximum transfer of energy of the AOTBF, which occurs for the LP_{01}–LP_{13} intermodal coupling when applying an RF signal of 1.642126 MHz and 33 V, as seen in Fig. 2(b). The measured optical spectrum for the laser emission is depicted in Fig. 4(a). The laser emission is centered at 1915.33 nm, in agreement with the calibration of the AOTBF, exhibiting a 3-dB
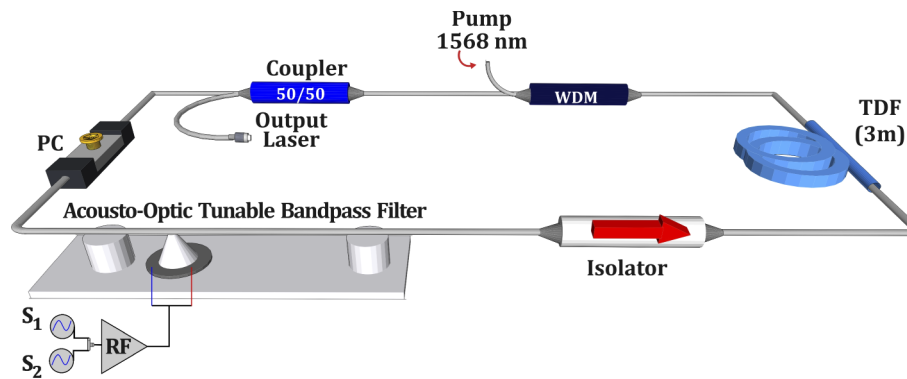
Fig. 3. Experimental setup of the all-fiber thulium-doped fiber.

optical bandwidth of 55 pm and a signal-to-noise ratio (SNR) higher than 60 dB. For this measurement, the spectrum was fixed to a peak power value of 0 dBm, however, higher output power is achievable with the present scheme. Figure 4(b) shows the output power dependence as a function of launched pump power. The laser output increases linearly after reaching the threshold of 200 mW, a maximum output power of 367 mW is achieved at the highest pump power. The slope efficiency for this laser is measured as 23.69%. The tunable characteristics of laser emission are presented in Fig. 4(c); we can point out that there is a perfect matching between the wavelength of the filter transmission peak, for the different modes and frequencies (see Fig. 2(d)), and the laser emission wavelength. The LP_{01}–LP_{13} intermodal coupling can be tuned over a wide span of optical wavelengths, from 1757.6 to 1940.5 nm, corresponding to an acoustic wave frequency range from 2.082226 to 1.584926 MHz, respectively. Laser emission below 1757.6 nm was not possible to observe because of the combination of low gain of thulium-doped fiber and relatively low transmittance of the AOTBF. The frequency response of piezoelectric disks is not flat and this limits the bandwidth operation of the AOTBF. Laser lines of the LP_{01}–LP_{13} intermodal coupling possess the advantages of narrow linewidth of at least 55 pm, high SNR greater than 45 dB, and fine tuning at a rate of -0.367 nm/kHz.

In order to demonstrate additional tuning capacities, the AOTBF is operated taking into account the remaining set of intermodal couplings, LP_{01}–LP_{11}, LP_{01}–LP_{12} and LP_{01}–LP_{14}. For this purpose, the acoustic wave frequency is used to select the desired intermodal coupling and the PC, connected previous to the filter, is used to maximize the desired peak transmission. The maximum efficiency is obtained when light is polarized with the same vibration plane of the acoustic wave [44]. Thus, the PC adjusts the polarization state in the cavity previous to the AOTBF and controls the bandpass transmission efficiency. The laser emission spectra for the three intermodal couplings are illustrated in Fig. 5. In a similar way than the presented results in Fig. 4(c), the tuning characteristics of the laser wavelengths are in agreement with the calibration of the AOTBF, see Fig. 2(d). They were fixed to a peak power of 0 dBm in the spectrum, maintaining a SNR higher that 45 dB and 3 dB bandwidths of around 50 pm in most of the presented cases. The tuning range is measured as 170.9, 163.29 and 193.61 nm for the LP_{01}–LP_{11}, LP_{01}–LP_{12} and LP_{01}–LP_{14} resonances, respectively. Considering all the resonant couplings, the shortest wavelength emission appears at 1757.6 nm, whereas the longest wavelength is achieved at 1969.1 nm, yielding a total tuning range of 211.5 nm. If we compare this result with recent published works [45–48], this tuning range is the largest observed to the best of our knowledge. It is worth highlighting the narrow linewidth generation, the fine-tuning range, and the robustness of the filter device that allows a precise control of laser emission.
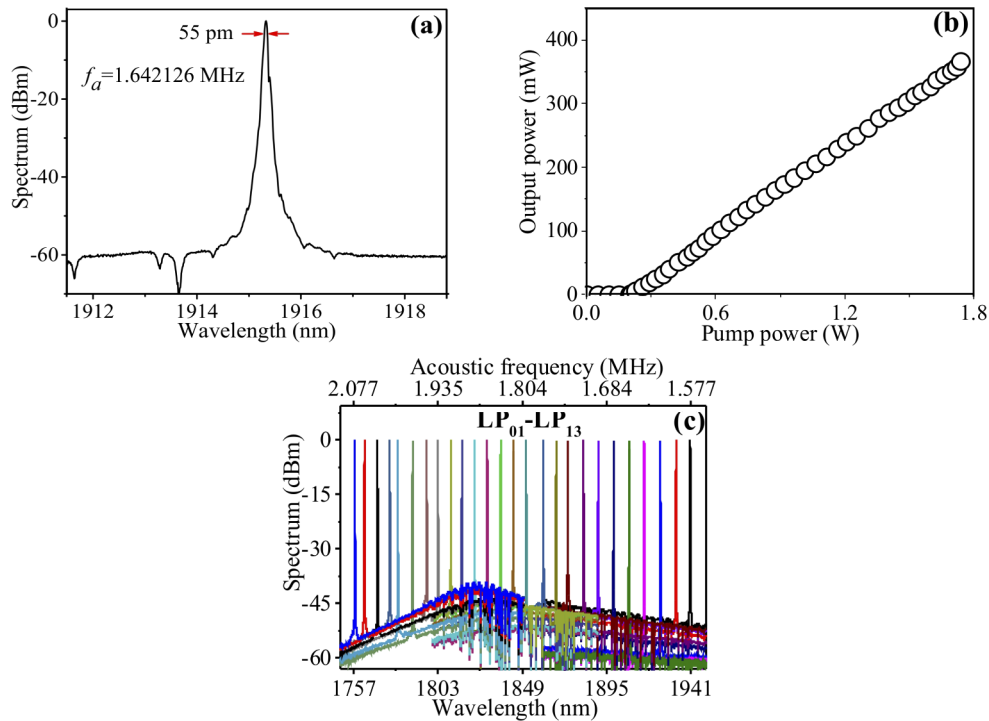
Fig. 4. (a) Optical spectrum of the single-wavelength laser at the acoustic frequency of 1.642126 MHz. (b) Dependence of the output power as a function of the launched pump power. (c) Tunability of the single wavelength laser operation for the LP_{01}–LP_{13} intermodal coupling.

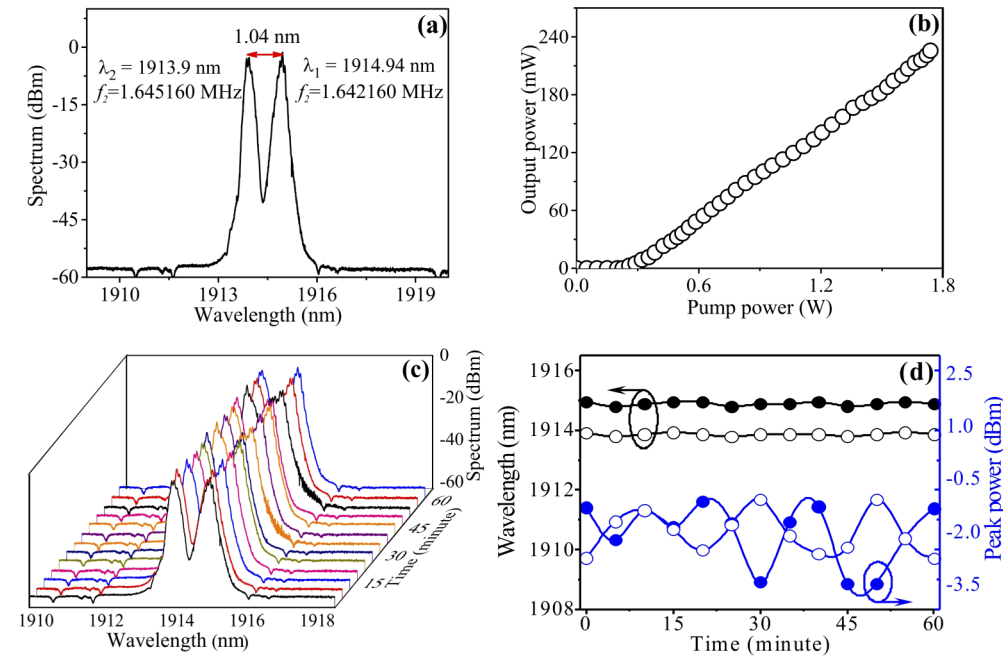### 3.2. *Dual-wavelength operation*

One interesting property of the present scheme is the ability to generate a dual-wavelength emission by implementing simultaneously two electrical signal sources into the AOTBF. In this way, each laser line of the dual-wavelength emission is controlled by a single signal source, in such a way that properties of the dual-wavelength emission, such as amplitude, spectral position and wavelength separation, are controlled dynamically by adjustments of the input acoustic signals. The first set of experiments was performed in order to determine the minimum wavelength spacing. For this goal, one of the RF signal is selected for the case of strongest intermodal coupling, which occurs at the acoustic frequency of 1.64216 MHz (f_1) and produces a laser line located at the resonant optical wavelength of 1914.94 nm, whereas the other acoustic frequency (f_2) was selected close enough to f_1 to achieve a stable dual-wavelength operation. The minimum wavelength spacing is obtained when f_2 reaches the value of 1.64516 MHz, producing a laser line at 1913.9 nm. Figure 6(a) illustrates the spectrum of dual-wavelength emission for the case of minimum wavelength spacing. The measured full-width at half maximum (FWHM) for the 1913.9 and 1914.94 nm laser lines is 129 and 56 pm, respectively. Both laser lines were adjusted via the amplitude of their respective acoustic wave to a peak power spectrum of 0 dBm, where a SNR higher than 56 dB is observed. The separation between the wavelengths of the laser emission spectra is measured as 1.04 nm. This last result could be considered as the limit in wavelength spacing for a stable operation, and it coincides with half the bandwidth of the AOTBF, see Fig. 2(c). The output power dependence as a function of launched pump power is shown in Fig. 6(b). The maximum output power for the dual-wavelength emission was 225.7 mW,
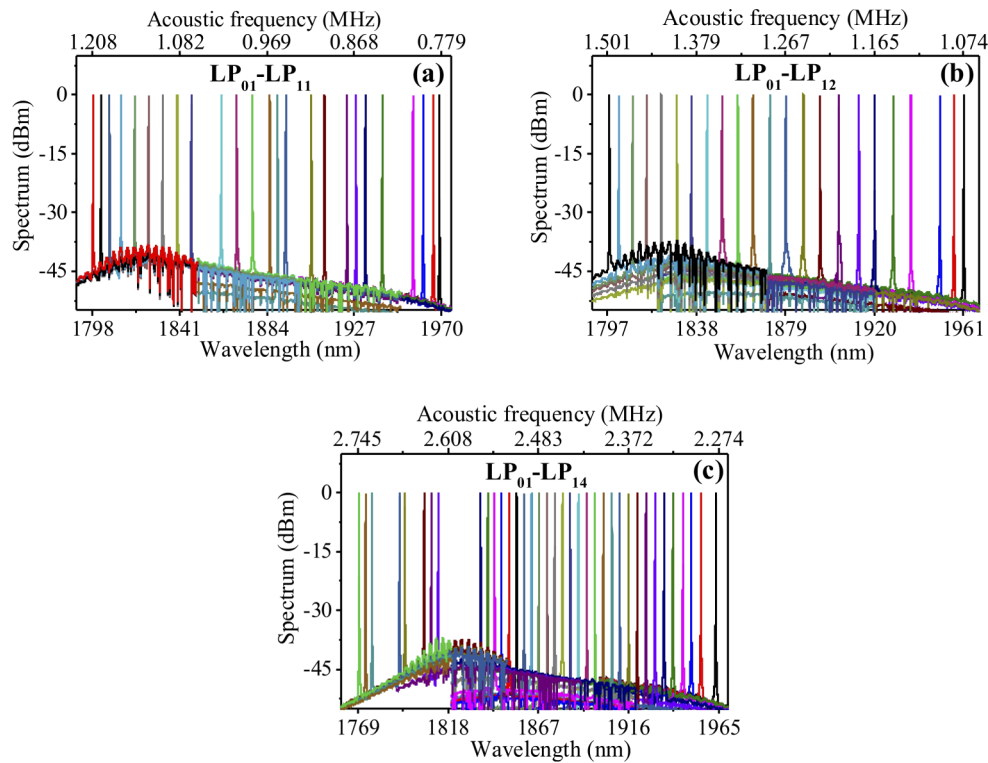
Fig. 5. Tunability of the single wavelength laser operation as a function of the acoustic wave frequency for (a) LP_{01}–LP_{11}, (b) LP_{01}–LP_{12}, (c) LP_{01}–LP_{14} intermodal couplings.

showing a slope efficiency of 15.05%. The stability of dual-wavelength operation is evaluated by monitoring the spectrum recorded every 5 minutes for total time of 1 hour under a fixed pump power of 0.568 W, as depicted in Fig. 6(c). The intensity and central wavelengths have fluctuations of less than 0.15 nm and 2.3 dB, as indicated in Fig. 6(d). When the laser is operated with a small wavelength separation, the power fluctuations (see Fig. 6(d)) appear to be produced by gain competition, since in this case a power increase in one wavelength can be correlated with a decrease of power in the other wavelength.

The case of maximum wavelength spacing is shown in Fig. 7. Simultaneous laser lines at 1802.67 and 1932.75 nm were obtained when the PD is biased with RF signals of 1.942126 and 1.602260 MHz, respectively. A maximum wavelength separation of 130.08 nm is measured. The corresponding 3-dB bandwidths of the shortest and longest wavelengths were measured as 62.64 and 52 pm, with corresponding SNRs of 47.6 and 52 dB, respectively. The total output power of the dual-wavelength fiber laser (DWFL) as a function of the pump power is illustrated in Fig. 7(b). In order to study the stability of the DWFL at room temperature, the pump power of the laser is fixed at 0.593 W, then the optical spectrum was repeatedly measured in 60 minutes with intervals of 5 minutes, as shown in Fig. 7(c). Figure 7(d) shows the fluctuations of the output power and wavelength variations in dual-wavelength operation. The maximum peak power fluctuation of both wavelengths was less than 5.8 dB and the center wavelength shift of both wavelengths was less than 0.27 nm. When the laser is operated with a large wavelength separation, then power fluctuations are not dominated by gain competition, but other mechanisms, such as pump power fluctuations, thermal effects in the piezoelectric transducer, vibrations of the mechanical elements and variations in room temperature. These results demonstrate a stable and reasonably
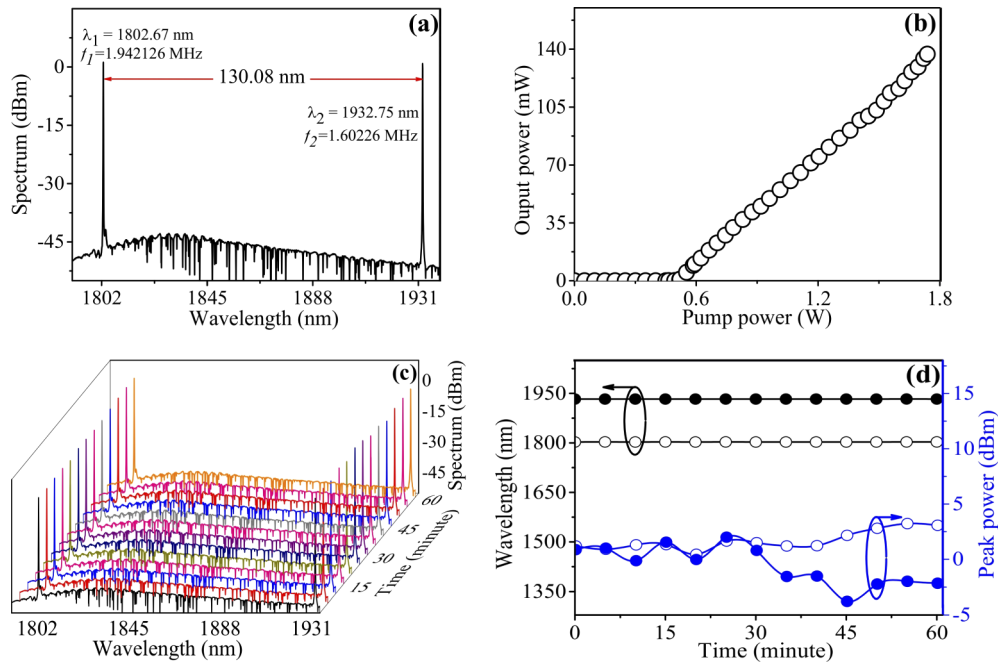
Fig. 6. Characteristics of dual-wavelength laser operation for minimum wavelength spacing. (a) Optical spectrum at pump power of 0.568 W. (b) Output power as a function of pump power. (c) Stability measurement. (d) Fluctuations of the output peak powers and the center wavelengths.

uniform dual-wavelength operation. However, if an improved stable emission is required, then an active feedback could be implemented in order to readjust in real time the amplitude of the radio frequency signals that drive the piezoelectric transducer, in order to provide an independent control of the cavity losses for each wavelength.

Another interesting feature of the present scheme is the ability of independent tuning of laser lines. This characteristic is presented in Fig. 8, where one of the RF signals is fixed throughout the measurement process, and the other source is adjusted to tune the wavelength emission. Figure 8(a) shows the case of maintaining frequency f_1 fixed at 1.942126 MHz, while frequency f_2 is varied from the initial value of 1.602260 MHz towards f_1. The laser lines generated at this point, λ_1 and λ_2 are located at initial values of 1802.67 and 1932.8 nm, respectively, with a wavelength separation of 130.13 nm. For tuning of λ_2, the frequency f_2 was varied in steps of ~ 50 kHz, producing the shift of λ_2 from 1932.8 to 1806.06 nm. A maximum peak power difference of 1.45 dB was measured over the entire tuning process of 126.74 nm. The arrow in Fig. 8(a) shows the tuning direction of λ_2 and the upper axis indicates the frequency applied to the PD. The estimated SNR was measured as at least 44.5 dB for all the presented laser lines. A reverse operation is also observed after returning λ_1 and λ_2 to the initial positions, as shown in Fig. 8(b). In this case, λ_2 remains fixed at 1932.75 nm and λ_1 shifts to longer wavelengths. By applying step increments of 40 kHz, one observes a tuning of λ_1 from 1802.67 to 1926.18 nm. A maximum peak power difference of 1.7 dB and a minimum wavelength separation of 6.57 nm were measured between tuned lines. The arrow in Fig. 8(b) indicates the tuning direction of λ_2. In both cases, with the goal of balancing the cavity loss or gain, it was necessary to adjust the voltage applied to the piezoelectric disk (V_{PD}) in order to regulate the peak intensities of λ_1 and λ_2. V_{PD} was varied in a range between 17.4 and 37.6 V in the previous experiments. It is worth mentioning that in our present setup voltage values higher than 40 V degrade the response of the

Fig. 7. Characteristics of dual-wavelength laser operation for maximum wavelength spacing. (a) Optical spectrum at pump power of 0.593 W. (b) output power as a function of pump power. (c) Stability measurement. (d) Fluctuations of the output power and the center wavelength.

piezoelectric disk due to an excessive heating. Thus, our experiments were carried out using a maximum voltage of 37.6 V, where a stable and linear response of the piezoelectric was observed.
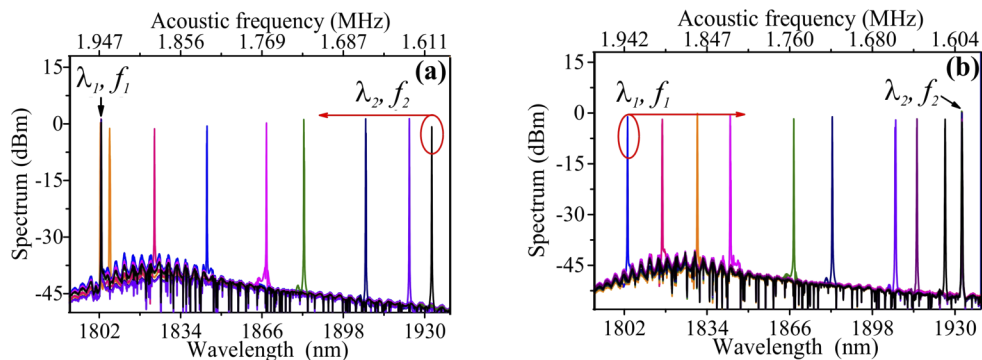
Fig. 8. Tunability of the dual-wavelength fiber laser. (a) Wavelength tuning of λ_2 while λ_1 remains fixed, and (b) wavelength tuning of λ_1 while λ_2 remains fixed. λ_1 and λ_2 are located at initial wavelength values of 1802.67 and 1932.8 nm, corresponding to acoustic frequencies f_1 of 1.942126 MHz and f_2 of 1.602260 MHz, respectively.

Based on the previous results, the proposed scheme demonstrates a versatile operation that give rise to stable, widely tunable and narrow linewidth laser emissions. In addition, due to the ability of the AOTBF to be operated by using two simultaneous input signals, it permits an independent tuning of each of the laser lines that is controlled via the amplitude and frequency of

the acoustic signals. Compared to recently reported widely tunable dual-wavelength fiber lasers [12,14,49], our scheme provides full electronic control and fast response, since it avoids thermal and mechanical devices. Therefore, the AOTBF could be considered a reliable fiber-optic device to perform a tight control over the cavity parameters and provides a high degree of repeatability.

4. Conclusion

A tunable single- and dual-wavelength TDFL based on an in-fiber AOTBF is experimentally demonstrated. Tuning characteristics of laser emissions were controlled via the bandpass transmission of the AOTBF. The AOTBF was especially designed to be operated in the thulium emission band, and takes advantage of the AO effect when a flexural acoustic wave propagates along the optical fiber. The filter produces a bandpass transmission that depends on the amplitude and frequency of the acoustic wave, providing a minimum insertion loss of 4.75 dB with a strong suppression of light by at least 20 dB over a range from 1820.41 to 1928.41 nm. A 3-dB optical bandwidth of 2.04 nm was measured for the AOTBF. Based on this approach, single-wavelength operation exhibits a total tuning range of 211.5 nm, extending from 1757.6 to 1969.1 nm, with characteristics of narrow linewidth (50 pm) and high SNR (60 dB). Moreover, by operating the AOTBF with two independent input RF signals, a dual-wavelength emission with independently tunable lines was demonstrated. The minimum and maximum wavelength separation was measured as 1.04 and 130.08 nm, respectively. A total tuning range of 130.08 nm that extends from 1802.67 to 1932.75 nm was achieved for any of the two lines, with a maximal peak power difference of 2 dB. The laser performs a long-term stability over a period of hours, which is mainly attributed to the stable characteristics of the AOTBF. The proposed scheme is useful and convenient for practical applications, it preserves the simplicity and robustness required in all-fiber arrangements.

Funding

Disclosures

The authors declare no conflicts of interest.

References

1. M. Y. Jeon, N. Kim, J. Shin, J. S. Jeong, S. P. Han, C. W. Lee, Y. A. Leem, D. S. Yee, H. S. Chun, and K. H. Park, "Widely tunable dual-wavelength Er^{3+}-doped fiber laser for tunable continuous-wave terahertz radiation," Opt. Express **18**(12), 12291–12297 (2010).
2. H. Ahmad, F. D. Muhammad, C. H. Pua, and K. Thambiratnam, "Dual-wavelength fiber lasers for the optical generation of microwave and terahertz radiation," IEEE J. Sel. Top. Quantum Electron. **20**(5), 166–173 (2014).
3. T. Tiess, M. Becker, M. Rothhardt, H. Bartelt, and M. Jäger, "Independently tunable dual-wavelength fiber oscillator with synchronized pulsed emission based on a theta ring cavity and a fiber Bragg grating array," Opt. Express **25**(22), 26393–26404 (2017).
4. T. Gottschall, T. Meyer, M. Baumgartl, C. Jauregui, M. Schmitt, J. Popp, J. Limpert, and A. Tunnermann, "Fiber-based light sources for biomedical applications of coherent anti-Stokes Raman scattering microscopy," Laser Photonics Rev. **9**(5), 435–451 (2015).
5. D. Liu, N. Q. Ngo, S. C. Tjin, and X. Dong, "A dual-wavelength fiber laser sensor system for measurement of temperature and strain," IEEE Photonics Technol. Lett. **19**(15), 1148–1150 (2007).
6. Z. R. Lin, C. K. Liu, and G. Keiser, "Tunable dual-wavelength erbium-doped fiber ring laser covering both C-band and L-band for high-speed communications," Optik **123**(1), 46–48 (2012).
7. W. J. Peng, F. P. Yan, Q. Li, S. Liu, T. Feng, S. Y. Tan, and S. C. Feng, "1.94 µm switchable dual-wavelength Tm3+ fiber laser employing high-birefringence fiber Bragg grating," Appl. Opt. **52**(19), 4601–4607 (2013).
8. S. Liu, F. Yan, W. Peng, T. Feng, Z. Dong, and G. Chang, "Tunable dual-wavelength thulium-doped fiber laser by employing a HB-FBG," IEEE Photonics Technol. Lett. **26**(18), 1809–1812 (2014).

9. Y. Ding, Y. Liu, Y. Qi, L. Zhang, B. Guo, R. Wang, J. Zhou, and G. Chen, "Dual-wavelength narrow-linewidth linearly polarized seed source and stimulated Brillouin sacattering suppression in its high-power fiber amplification," Appl. Opt. **54**(22), 6616–6621 (2015).

10. S. Wang, P. Lu, S. Zhao, D. Liu, W. Yang, and J. Zhang, "2-μm switchable dual-wavelength fiber laser with cascaded filter structure based on dual-channel Mach-Zehnder interferometer and spatial mode beating effect," Appl. Phys. B **117**(2), 563–569 (2014).

11. M. R. K. Soltanian, H. Ahmad, A. Khodaie, I. S. Amiri, M. F. Ismail, and S. W. Harun, "A stable dual wavelength thulium-doped fiber laser at 1.9 μm using photonic crystal fiber," Sci. Rep. **5**(1), 14537 (2015).

12. B. Ibarra-Escamilla, E. Bravo-Huerta, M. Durán-Sánchez, R. I. Álvarez-Tamayo, B. Posada-Ramírez, P. Prieto-Cortés, J. E. Antonio-López, H. Santiago-Hernández, J. G. Aguilar-Soto, and E. A. Kuzin, "Dual-wavelength thulium-doped fiber laser with separate wavelengths selection based on a two mmi filters configuration," Laser Phys. **28**(9), 095107 (2018).

13. W. Ma, T. Wang, P. Zhang, J. Han, and J. Zhang, "Widely tunable multiwavelength thulium-doped fiber laser using a fiber interferometer and a tunable spatial mode-beating filter," Appl. Opt. **54**(12), 3786–3791 (2015).

14. H. Ahmad, M. Z. Samion, K. Thambiratnam, and M. Yasin, "Widely tunable dual-wavelength thulium-doped fiber laser operating in 1.8-2.0 mm region," Optik **179**, 76–81 (2019).

15. X. Ma, S. Luo, and D. Chen, "Switchable and tunable thulium-doped fiber laser incorporating a Sagnac loop mirror," Appl. Opt. **53**(20), 4382–4385 (2014).

16. T. Wang, W. Ma, P. Zhang, Q. Jia, J. Zhang, and H. Jiang, "Multi-wavelength narrow linewidth thulium-doped fiber laser operating at 1.9 μm using a tunable Sagnac fiber period filter," J. Opt. **44**(3), 210–214 (2015).

17. W. He, L. Zhu, M. Dong, and F. Luo, "Tunable and switchable thulium-doped fiber laser utilizing Sagnac loops incorporating two-stage polarization maintaining fibers," Opt. Fiber Technol. **29**, 65–69 (2016).

18. H. Wei, Z. Lianqing, D. Mingli, and L. Fei, "Tuneable and stable multi-wavelength thuliumdoped ring-cavity fibre laser based on Sagnac loop and Mach-Zehnder filter utilizing thin-core fibre," Laser Phys. **26**(12), 125102 (2016).

19. W. Ma, T. Wang, Y. Su, Y. Zhang, P. Liu, Q. Jia, P. Zhang, and H. Jiang, "Wavelength-spacing switchable dual-wavelength single longitudinal mode thulium-doped fiber laser at 1.9 μm," IEEE Photonics J. **8**(6), 1–8 (2016).

20. K. S. Hong, H. C. Park, I. K. Hwang, W. Jin, J. Ju, D. I. Yeom, and B. Y. Kim, "1000 nm tunable acousto-optic filter based on photonic crystal fiber," Appl. Phys. Lett. **92**(3), 031110 (2008).

21. S. D. Lim, K. J. Park, S. H. Eom, J. M. Jeong, B. Y. Kim, and S. B. Lee, "Ultrawidely tunable single-mode fiber acousto-optic filter," Opt. Lett. **36**(7), 1101–1103 (2011).

22. W. D. Zhang, F. Gao, F. Bo, Q. Wu, G. Q. Zhang, and J. J. Xu, "All-fiber acousto-optic tunable notch filter with a fiber winding driven by a cuneal acoustic transducer," Opt. Lett. **36**(2), 271–273 (2011).

23. W. D. Zhang, L. G. Huang, F. Gao, F. Bo, G. Q. Zhang, and J. J. Xu, "Tunable broadband light coupler based on two parallel all-fiber acousto-optic tunable filters," Opt. Express **21**(14), 16621–16628 (2013).

24. K. J. Lee, D. I. Yeom, and B. Y. Kim, "Narrowband, polarization insensitive all-fiber acousto-optic tunable bandpass filter," Opt. Express **15**(6), 2987–2992 (2007).

25. W. Zhang, L. Huang, F. Gao, F. Bo, L. Xuan, G. Zhang, and J. Xu, "Tunable add/drop channel coupler based on an acousto-optic tunable filter and a tapered fiber," Opt. Lett. **37**(7), 1241–1243 (2012).

26. C. Cuadrado Laborde, M. Bello Jiménez, A. Díez, J. L. Cruz, and M. V. Andrés, "Long-cavity all-fiber ring laser actively mode locked with an in-fiber bandpass acousto-optic modulator," Opt. Lett. **39**(1), 68–71 (2014).

27. H. Zhang, S. Kang, B. Liu, H. Dong, and Y. Miao, "All-Fiber Acousto-Optic Tunable Bandpass Filter Based on a Lateral Offset Fiber Splicing Structure," IEEE Photonics J. **7**(1), 1–12 (2015).

28. L. Huang, X. Song, P. Chang, W. Peng, W. Zhang, F. Gao, F. Bo, G. Zhang, and J. Xu, "All-fiber tunable laser based on an acousto-optic tunable filter and a tapered fiber," Opt. Express **24**(7), 7449–7455 (2016).

29. G. Ramírez Meléndez, M. Bello Jiménez, O. Pottiez, and M. V. Andrés, "Improved all-fiber acousto-optic tunable bandpass filter," IEEE Photonics Technol. Lett. **29**(12), 1015–1018 (2017).

30. L. Huang, W. Zhang, Y. Li, H. Han, X. Li, P. Chang, F. Gao, G. Zhang, L. Gao, and T. Zhu, "Acousto-optic tunable bandpass filter based on acoustic-flexural-wave-induced fiber birefringence," Opt. Lett. **43**(21), 5431–5434 (2018).

31. W. Zhang, L. Huang, K. Wei, P. Li, B. Jiang, D. Mao, F. Gao, T. Mei, G. Zhang, and J. Zhao, "Cylindrical vector beam generation in fiber with mode selectivity and wavelength tunability over broadband by acoustic flexural wave," Opt. Express **24**(10), 10376–10384 (2016).

32. L. Carrión Higueras, E. P. Alcusa Sáez, A. Díez, and M. V. Andrés, "All-fiber laser with intracavity acousto-optic dynamic mode converter for efficient generation of radially polarized cylindrical vector beams," IEEE Photonics J. **9**(1), 1 (2016).

33. K. Wei, W. Zhang, L. Huang, D. Mao, F. Gao, T. Mei, and J. Zhao, "Generation of cylindrical vector beams and optical vortex by two acoustically induced fiber gratings with orthogonal vibration directions," Opt. Express **25**(3), 2733–2741 (2017).

34. J. Lu, L. Meng, F. Shi, X. Liu, Z. Luo, P. Yan, L. Huang, F. Pang, T. Wang, X. Zeng, and P. Zhou, "Dynamic mode-switchable optical vortex beams using acousto-optic mode converter," Opt. Lett. **43**(23), 5841–5844 (2018).

35. X. Zhang, W. Zhang, C. Li, D. Mao, F. Gao, L. Huang, D. Yang, T. Mei, and J. Zhao, "All-fiber cylindrical vector beams laser based on an acoustically-induced fiber grating," J. Opt. **20**(7), 075608 (2018).

36. E. P. Alcusa-Sáez, A. Díez, M. González-Herráez, and M. V. Andrés, "Time-resolved acousto-optic interaction in single-mode optical fibers: Characterization of axial nonuniformities at the nanometer scale," Opt. Lett. **39**(6), 1437–1440 (2014).

37. L. Pei, C. Liu, J. Li, J. Zheng, S. Yu, and L. Wu, "Highly Sensitive Axial Strain Fiber Laser Sensor Based on All-Fiber Acousto-Optic Tunable Filter," IEEE Photonics Technol. Lett. **26**(24), 2430–2433 (2014).

38. E. P. Alcusa Sáez, A. Díez, M. González Herráez, and M. V. Andrés, "Improved time-resolved acousto-optic technique for optical fiber analysis of axial non-uniformities by using edge interrogation," Opt. Express **23**(6), 7345–7350 (2015).

39. E. P. Alcusa-Sáez, A. Díez, and M. V. Andrés, "Accurate mode characterization of two-mode optical fibers by in-fiber acousto-optics," Opt. Express **24**(5), 4899–4905 (2016).

40. E. Rivera-Pérez, A. Carrascosa, A. Díez, E. P. Alcusa-Sáez, and M. V. Andrés, "An approach to the measurement of the nonlinear refractive index of very short lengths of optical fibers," Appl. Phys. Lett. **113**(1), 011108 (2018).

41. E. Hernández Escobar, M. Bello Jiménez, A. Camarillo Avilés, R. López Estopier, O. Pottiez, M. V. Hernández Arriaga, M. Durán Sánchez, B. Ibarra Escamilla, and M. V. Andrés, "Broadband tuning of a long-cavity all-fiber mode-locked thulium-doped fiber laser using an acousto-optic bandpass filter," Opt. Lett. **44**(17), 4183–4186 (2019).

42. H. E. Engan, B. Y. Kim, J. N. Blake, and H. J. Shaw, "Propagation and optical interaction of guided acoustic waves in two-mode optical fibers," J. Lightwave Technol. **6**(3), 428–436 (1988).

43. L. S. Rothman, I. E. Gordon, Y. Babikov, A. Barbe, D. Chris Benner, P. F. Bernath, M. Birk, L. Bizzocchi, V. Boudon, L. R. Brown, A. Campargue, K. Chance, E. A. Cohen, L. H. Coudert, V. M. Devi, B. J. Drouin, A. Fayt, J. M. Flaud, R. R. Gamache, J. J. Harrison, J. M. Hartmann, C. Hill, J. T. Hodges, D. Jacquemart, A. Jolly, J. Lamouroux, R. J. Le Roy, G. Li, D. A. Long, O. M. Lyulin, C. J. Mackie, S. T. Massie, S. Mikhailenko, H. S. P. Müller, O. V. Naumenko, A. V. Nikitin, J. Orphal, V. Perevalov, A. Perrin, E. R. Polovtseva, C. Richard, M. A. H. Smith, E. Starikova, K. Sung, S. Tashkun, J. Tennyson, G. C. Toon, V. G. Tyuterev, and G. Wagner, "The HITRAN 2012 molecular spectroscopic database," J. Quant. Spectrosc. Radiat. Transfer **130**, 4–50 (2013).

44. T. A. Birks, P. St. Russell, and D. O. Culverhouse, "The acousto-optic effect in single-mode fiber tapers and couplers," J. Lightwave Technol. **14**(11), 2519–2529 (1996).

45. Y. Wei, K. Hu, B. Sun, and T. Wang, "All-fiber widely wavelength-tunable thulium-doped fiber ring laser incorporating a Fabry-Perot filter," Laser Phys. **22**(4), 770–773 (2012).

46. Z. Li, S. U. Alam, Y. Jung, A. M. Heidt, and D. J. Richardson, "All-fiber, ultra-wideband tunable laser at 2 μm," Opt. Lett. **38**(22), 4739–4742 (2013).

47. Z. Li, A. M. Heidt, J. M. O. Daniel, Y. Jung, S. U. Alam, and D. J. Richardson, "Thulium-doped fiber amplifier for optical communications at 2 μm," Opt. Express **21**(8), 9289–9297 (2013).

48. X. Ma, D. Chen, Q. Shi, G. Feng, and J. Yang, "Widely tunable thulium-doped fiber laser based on multimode interference with a large no-core fiber," J. Lightwave Technol. **32**(19), 3234–3238 (2014).

49. M. Wang, Y. Huang, L. Yu, Z. Song, D. Liang, and S. Ruan, "Multiwavelength thulium-doped fiber laser using a micro fiber-optic Fabry–Perot interferometer," IEEE Photonics J. **10**(4), 1–8 (2018).